Scientia Iranica B (2013) 20(5), 1508–1516

Sharif University of Technology
Scientia Iranica
Transactions B: Mechanical Engineering
www.scientiairanica.com

Numerical investigation on the external compressible flow around NACA m1 and NACA 0015 airfoils

S. Akbarpour[a] and M. Ghorbani[b,1,*]

a. *Department of Mechanical Engineering, Sahand University of Technology, Tabriz, Iran.*
b. *Center for CFD Studies on Heat Engines, Cavitational Flows and Petroleum Industries, Department of Mechanical Engineering, University of Tabriz, Tabriz, Iran.*

Received 6 May 2012; received in revised form 28 January 2013; accepted 14 May 2013

KEYWORDS
Airfoil;
Drag coefficient;
k-ε model;
Mach number;
Spalart-Almaras model.

Abstract. The importance of the external flows around the airfoils became serious when the airplanes with high velocity crashed due to passing the critical Mach number. These events caused the significance of the effects of the Mach number on the drag and lift force to become clear. In this paper, the modeling of two standard airfoils for different angles of attack and various Mach numbers are. The external flows around the airfoil are solved by two turbulence models which are Splalart-Alamaras and k-ε models. Both of the airfoils have been modeled for Mach numbers from 0.8 to 1.2 and angle of attacks of 0 and 4 degrees. The pressure and drag coefficients, pressure force for both top and bottom walls of the airfoils, are calculated by using the Spalart-Almaras and k-ε models. The results show that the drag coefficient increases intensively when the Mach number is equal to one, then for a determined Mach number, the drag coefficient is stable. The drag force and coefficient of the two above turbulence models in different Mach numbers are investigated, and the location of the shock wave phenomenon for the airfoils NACA m1 and NACA 0015, with different angle of attacks, is studied.

1. Introduction

Numerical analysis of airfoils has a significant effect on the development of engineering and scientific applications of flows around the airfoils and studying different phenomena such as shock wave, lift and drag coefficients and shear tension around it. Investigation of the flows around the airfoil is essential for designing and producing the airfoils and assessing their resistance against the external forces. Applied theory of subsonic flights with high velocity shows how the drag coefficient follows its ascending trend when the Mach number tends to one. The lift coefficient tracks its ascending trend to obtain its maximum value at Mach number equal to one. Lift coefficient has a finite value at Mach number equal to one and deals with one-dimensional phenomena such as vertical shock waves and channels flows in compressible flows. Therefore, study of compressible external flows, and investigation of the lift and drag coefficients, and force around the airfoils are essential. There are many models for analyzing and simulating the compressible external flows around the airfoils that are used to obtain the effects of Mach number and the flows around the airfoil on the physical and thermodynamic characteristics of the flows. A semi-discrete centered finite volume scheme is employed for analyzing an approximate eigenvalue by Eriksson and Rizzi [1]. They have adopted this analysis to transonic inviscid flow around an airfoil. Van Buuren et al. [2] numerically investigated an unstable condition of

1. *Present address: Mechatronics Engineering Program, Faculty of Engineering and Natural Sciences, Sabancı University.*
*. *Corresponding author. Tel.: +90 553 5526917,*
E-mail address: morteza@sabanciuniv.edu (M. Ghorbani).

inviscid compressible flow around an airfoil. They have found a physical unstable situation in the wake behind the airfoil by using the explicit method. They have also mentioned that a linear stability theory can anticipate this unstable condition. Mittal [3] has studied an unsteady viscous compressible flow around a NACA 0012 airfoil by using finite element computation. He has found that the flow around the airfoil is unsteady in the case of the width of 8.5. When the Mach number is equal to 0.85, the Reynolds number is equal to 10000 and the angle of attack is equal to zero. Olejniezak and Lyrintzis [4] have designed an airfoil in subcritical flow. They have illustrated the optimization of the drag by Squire - Young drag formula. They have shown in their optimized airfoil, more lift and less drag generation for compressible and incompressible flows in comparison with other airfoils. The development and simulation of the flow control devices design is of great importance in studying the performance of the airfoils in different situations, and investigating significant phenomena such as lift and drag coefficients [5]. Qin xuguo et al. [6] have simulated two-dimensional airfoil and investigated the lift and drag coefficients by using the Finite-Volume method. Mittal and Saxena [7] have investigated the effects of decreasing and increasing the angle of attack on the separation point. They have tried to analyze and calculate the two-dimensional, incompressible ($M = 0.3$) flows around the NACA 0012 airfoil. The effects of various angles of attack on the lift and drag coefficients have also been studied at the same condition. Raja Kumar and Ravindran [8] have simulated NACA 4410 and NACA 2415 airfoils in order to design a wind turbine. The performance of the airfoils has been discussed at different conditions. They have investigated at different conditions, and also investigated the effects of the angle of attack on wind turbines to obtain the size of the router, and have tried to improve the geometry of the blades in the wind turbines. Hua Shan et al. [9] investigated the direct numerical simulation of flow separation around a NACA 0012 airfoil with an attack angle of 40 and a Reynolds number of 105. They have found that no external disturbances are introduced and the vortex shedding from the separated shear layer is related to the Kelvin-Helmholtz instability. Y. Zhou et al. [10] studied the fluid forces on a very low Reynolds number airfoil. They measured the forces by using a load cell, and the dependence of the forces on both attack angle, and Rec is revealed in this study. They have developed a theoretical analysis to predict and clarify the observed dependence of the mean lift and drag on the attack angle. Ghadimi and Rostami [11] investigated the aerodynamic analysis of the boundary layer region of symmetric airfoils. They have analyzed the amounts of drag and lift forces of the airfoil in viscous flows, and also studied the effects of variation of the Reynolds number and angle of attack. They have found that the motion at ground proximity is the cause of some changes in boundary layer characteristics. Wang and Ingham [12] investigated numerically the dynamic stall of low Reynolds number flow around airfoils, and showed that CFD prediction indicates well the vortex-shedding flow surface; the results agree well with the experimental data, except when the blade is at a very high angle of attack. Yao et al. [13] simulated the aerodynamic performance of NACA 0018, and discussed and compared the lift and drag coefficient of the airfoil under different turbulence models. Their calculation results are a reference for research and development of airfoils. Shi et al. [14] studied experimentally the flow around a bio-inspired airfoil at Re = 2*103 and different angles of attacks, by using Particle Image Velocimetry (PIV). They analyzed the global properties of the fluid flow around two airfoils with different values of angle of attack. They also reported that there was not a significant variation of the global flow patterns at 00. They showed that the flow was massively separated at a large angle of attack in both airfoils, which is in concordance with our results. Medjroubi et al. [15] investigated the flow around a heaving airfoil by using high-order numerical simulation. They simulated the incompressible and viscous flows over a two-dimensional NACA0012 airfoil for different Reynolds numbers and angles of attack. They reported that the variation of the Reynolds number has not a significant effect on the flow form, but the force coefficients, as well as drag and viscous coefficients, increase by increasing the Reynolds number.

In this paper, the compressible flows around the two standard airfoils, which are NACA m1 and NACA 0015, have been simulated. The most important issue in turbulence models is to find out the calculation of eddy viscosity. The Spalart-Almaras model solves a transmission equation for a value which is obtained from kinematic turbulent viscosity [16]. The results of the static pressure, Mach number and drag coefficient at top and bottom walls of the airfoils have been extracted. The results of the drag coefficient show that its maximum value takes place when the Mach number tends to one, which is provided in all of the sections. The location of shock wave can be also extracted; to study the drag and pressure coefficients, the flows have been solved at different values of Mach number with angle of attack of 0 and 4 degrees as the important purpose of this paper. The results of this work have been compared with the experimental works that show a good agreement.

2. Numerical and physical modeling

2.1. Continuity equation

Continuity equation for steady state flows is calculated as:

$$\frac{\partial \rho}{\partial t} + \nabla.(\rho V) = 0. \tag{1}$$

For the steady state, density as a function of time is given by:

$$\frac{\partial \rho}{\partial t} = 0. \tag{2}$$

Therefore, the continuity equation for the steady state is obtained as:

$$\frac{\partial}{\partial x}(\rho u) + \frac{\partial}{\partial y}(\rho v) = 0. \tag{3}$$

2.2. Momentum equation

Momentum equation for two-dimensional steady flows is obtained as:

$$\vec{\nabla}.\left(\rho u \vec{V}\right) = -\frac{\partial p}{\partial x} + \rho f_x + (f_x)_{\text{viscose}}, \tag{4}$$

$$\vec{\nabla}.\left(\rho v \vec{V}\right) = -\frac{\partial p}{\partial y} + \rho f_y + (f_y)_{\text{viscose}}, \tag{5}$$

where ρ is density, and f_x and f_y are surface forces.

2.3. Energy equation

The energy equation for the steady state flows is given as:

$$\vec{\nabla}.\left[\rho\left(e + \frac{V^2}{2}\right)\vec{V}\right] = \rho\dot{q} - \vec{\nabla}.\left(P\vec{V}\right) + \rho\left(\vec{f}.\vec{V}\right) + \dot{Q} + \dot{W}, \tag{6}$$

where $(\dot{Q})$ and $(\dot{W})$ show the existence of the viscous and its effect on the energy equation. Eq. (6) is a partial differential equation which connects the variables of the flow field to each other at a specific point in the space [17].

2.4. Transport equation for the Spalart-Almaras model

Transport equation is obtained from the transported variable $(\tilde{\gamma})$ in Spalart-Almaras model as:

$$\frac{\partial}{\partial t}(\rho\tilde{\gamma}) + \frac{\partial}{\partial x_i}(\rho\tilde{\gamma}u_i) = G_\gamma + \frac{1}{\sigma_{\tilde{\gamma}}}\left[\frac{\partial}{\partial x_i}\left\{(\mu + \rho\tilde{\gamma})\frac{\partial\tilde{\gamma}}{\partial x_j}\right\} + C_{b2}\rho\left(\frac{\partial\tilde{\gamma}}{\partial x_j}\right)^2\right] - Y_\gamma + S_{\tilde{\gamma}}, \tag{7}$$

where G_γ is the turbulent viscosity generation, and Y_γ is the destruction of the turbulent viscosity which is occurred close to the wall, due to the viscous damping. $\sigma_{\tilde{\gamma}}$ and C_{b2} are the constant coefficients and equal respectively, to 0.67 and 0.622. γ is the molecular kinematic viscosity and $S_{\tilde{\gamma}}$ is user-define source term. The below equation is used for modeling of turbulent viscosity, which calculates the turbulent viscosity:

$$\mu_t = \rho\tilde{\gamma}f_{v1}, \tag{8}$$

where f_{v1} is a viscous damping function and is obtained as:

$$f_{v1} = \frac{X^3}{x^3 + C_{v1}^3}, \tag{9}$$

$$X = \frac{\tilde{\gamma}}{\gamma}. \tag{10}$$

C_{v1} is the constant coefficient and equal to 7.1. The Eqs. (11) and (12) are used to obtain the production term:

$$G_\gamma = C_{b1}\rho\tilde{S}\tilde{\gamma}, \tag{11}$$

$$\tilde{S} \equiv S + \frac{\tilde{\gamma}}{K^2 d^2}f_{v2}, \tag{12}$$

in which C_{b1} and K are constant coefficients and are: $C_{b1} = 0.1355$ and $K = 0.4187$. d is the distance from the wall and S is scalar measure of the deformation tensor. The below equations state how to calculate the turbulent destruction (Y_γ):

$$Y_\gamma = C_{w1}\rho f_w\left(\frac{\tilde{\gamma}}{d}\right)^2, \tag{13}$$

$$f_w = g\left[\frac{1 + C_{w3}^6}{g^6 + C_{w3}^6}\right]^{1/6}, \tag{14}$$

$$g = r + C_{w2}\left(r^6 - r\right), \tag{15}$$

$$r \equiv \frac{\tilde{\gamma}}{\tilde{S}K^2 d^2}, \tag{16}$$

in which C_{w1}, C_{w2} and C_{w3} are the constant coefficients, and $\tilde{S}$ is obtained from Eq. (12). The constant values are also obtained as:

$$C_{w1} = \frac{C_{b1}}{K^2} + \frac{(1 + C_{b2})}{\sigma_{\tilde{\gamma}}}. \tag{17}$$

By calculating the above equation, the value of C_{w1} is obtained as $C_{w1} = 3.2059$, and C_{w2} and C_{w3} are equal, respectively, to 0.3 and 2.0 [16].

2.5. k-ε standard model

The k-ε standard model is a semi-empirical model [18] which relies on the turbulence kinetic energy and its dissipation rate. It is supposed that the flow is completely turbulent in this model, and the molecular viscosity can be negligible. Therefore, this model is used for turbulent flows. Eqs. (18) and (19) show the transport equation for k-ε model.

$$\frac{\partial}{\partial t}(\rho k)+\frac{\partial}{\partial x_i}(\rho k u_i)=\frac{\partial}{\partial x_i}\left[\left(\mu+\frac{\mu_t}{\sigma_k}\right)\frac{\partial k}{\partial x_j}\right] + G_k + G_b - \rho\varepsilon - Y_M + S_k, \tag{18}$$

$$\frac{\partial}{\partial t}(\rho \varepsilon)+\frac{\partial}{\partial x_i}(\rho \varepsilon u_i)=\frac{\partial}{\partial x_i}\left[\left(\mu+\frac{\mu_t}{\sigma_\varepsilon}\right)\frac{\partial \varepsilon}{\partial x_j}\right] + C_{1\varepsilon}\frac{\varepsilon}{k} + (G_k + C_{3\varepsilon}G_b) - C_{2\varepsilon}\rho\frac{\varepsilon^2}{k} + S_\varepsilon, \tag{19}$$

in which G_k is the turbulent kinetic energy and Y_M is the contribution of the fluctuating dilation in compressible turbulence; $C_{1\varepsilon}$ and $C_{2\varepsilon}$ are constant coefficients which equal, respectively, to 1.44 and 1.92; σ_k and σ_ε are turbulent prandtl numbers for k and ε and equal, respectively, to 1 and 1.3. Likewise, μ_t is obtained as:

$$\mu_t = \rho C_\mu \frac{K^2}{\varepsilon}, \tag{20}$$

in which C_μ is equal to 0.09.

2.6. Loads on an airfoil

The pressure coefficient (C_p) is obtained from [15]:

$$C_p \equiv \frac{P-P_\infty}{q_\infty}. \tag{21}$$

q_∞ is the dynamic pressure and is obtained by:

$$q_\infty = \frac{1}{2}\rho_\infty V_\infty^2. \tag{22}$$

The dynamic pressure as a function of M_∞ is obtained as:

$$q_\infty = \frac{1}{2}\frac{\gamma q_\infty}{\gamma q_\infty}\rho_\infty V_\infty^2 = \frac{\gamma}{2}P_\infty\left[\frac{\rho_\infty}{\gamma P_\infty}\right]V_\infty^2. \tag{23}$$

And:

$$a_\infty^2 = \frac{\gamma P_\infty}{\rho_\infty}. \tag{24}$$

Therefor, q_∞ is obtained as:

$$q_\infty = \frac{\gamma}{2}P_\infty\frac{V_\infty^2}{a_\infty^2} = \frac{\gamma}{2}P_\infty M_\infty^2. \tag{25}$$

By considering Eqs. (21) and (25), C_p is obtained as:

$$C_p = \frac{2}{\gamma M_\infty^2}\left(\frac{P}{P_\infty}-1\right). \tag{26}$$

By supposing α as an angle of attack and C as a length of the airfoil, C_N and C_X are obtained as [19]:

$$C_N = \int_{x=0}^{x=C} (C_{P,\mathrm{low}} - C_{P,\mathrm{up}})\, d\left(\frac{x}{c}\right), \tag{27}$$

$$C_X = \int_{x=0}^{x=C}\left(C_{P,\mathrm{up}}\left(\frac{dY}{dX}\right)_{\mathrm{up}} - C_{P,\mathrm{low}}\left(\frac{dY}{dX}\right)_{\mathrm{low}}\right) d\left(\frac{x}{c}\right). \tag{28}$$

Finally drag and lift coefficients are obtained as:

$$C_D = C_X\cos\alpha + C_N\sin\alpha, \tag{29}$$

$$C_L = C_N\cos\alpha - C_X\sin\alpha. \tag{30}$$

2.7. The airfoil modeling

In this work, the airfoils NACA m1 and NACA 0015 [20] are simulated. The initial conditions and boundary conditions are described and the meshing of the airfoils is carried out. At the beginning of the modeling, the grid is studied and the problem is analyzed in ten, twenty and thirty times more than the airfoil length for grids, and the results are compared with each other, which show a good agreement in almost all of the grids. The airfoils are modeled in the steady state and the fluid around the airfoils is air. The boundary conditions for the airfoils are pressure far field. Sutherland equation is chosen for viscosity, due to compressible flow with high velocity and the variation of the viscosity at different temperature. k-ε and Spalart-Almaras are selected as models of viscosity, and the results are obtained for angles of attack of 0 and 4 degrees and Mach numbers from 0.8 to 1.2. The aim of this work is to find the drag coefficient and shock wave phenomenon by analyzing the compressible flows around the airfoils.

3. Results

The airfoils NACA m1 and NACA 0015 are investigated in different study fields after meshing. The grid study is carried out in different mesh scales and the domain is studied in 10, 20 and 30 times bigger than the length of the airfoil. The results are extracted and compared with experimental results in order to achieve the proper results. By selecting the suitable mesh, the results are compared to the two turbulent models which are k-ε and Spalart-Almaras. First of all, the pressure force is investigated for the airfoil NACA m1 for Spalart-Almaras and k-ε models in different Mach numbers, and angles of attack and finally the drag coefficients are investigated for the mentioned models. The obtained results show similar characteristics which illustrate good agreement with each other and experimental results.

3.1. Grid study

The lengths of the airfoils which are models are 1 m. The study fields of the domain around the airfoils are selected 10, 20 and 30 times bigger than the length of the airfoil NACA 0015 in order to choose the most appropriate study field for the airfoils ($M = 0.438$). Making a comparison between them, the study field of 20 times bigger than the length of the airfoil is chosen. The results of the drag coefficient for different domains are shown in Table 1. The results of the domains, which are 20 and 30 times bigger than the length of the airfoil, are close to each other. The domain, whose length is 20 times bigger than the length of the airfoil, is chosen due to less iterations and the convergence existing in drag coefficient.

Figure 1 shows the comparison of the drag coefficients between the models and the experimental results for the angle of attack of zero with respect to the Reynolds number, which are solved by S-A model. As seen in Figure 1, the trend of the numerical models is similar to the experimental results, and the numerical model has an error equal to 1.7 percent at Re=10000000. Figure 2 illustrates the drag coefficient with respect to the Reynolds number for different cases, for the angle of attack of 4 degree. According to this figure, results of this paper have a good agreement with the experimental results, and the numerical model has an error of 5.5 percent at Re=10000000. Therefore, the results show a good agreement with the experimental results [21].

Figure 3 shows the wall shear stress against their position of the airfoil NACA 0015, which indicates the exact location of the outbreak of the shock wave. This figure also shows the different values of the wall shear stress for top and bottom walls of the airfoil NACA 0015 against the position, and also illustrates that the shock wave phenomenon takes place at $X/C \approx 0.85$. It is also obvious that the values of the wall shear stress on the bottom wall are almost steady, and they do not have a significant change. Figure 4 shows the pressure coefficient of the top and bottom walls of the airfoil NACA 0015 with respect to the position. It also shows that the shock wave phenomenon is occurred at $X/C \approx 0.85$. As it is expected, the maximum pressure occurs at the location of the shock wave.

Table 1. The results of the drag coefficient for the airfoil NACA 0015 ($M = 0.438$, $\alpha = 0$).

	Dom.10	**Dom.20**	**Dom.30**	**Sheldahl et al.**
C_D	0.00778	0.00692	0.00691	0.0068

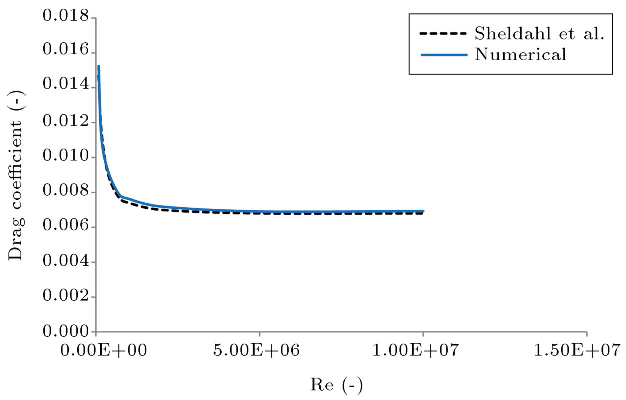

Figure 1. The variation of drag coefficient with respect to the Reynolds number ($\alpha = 0$).

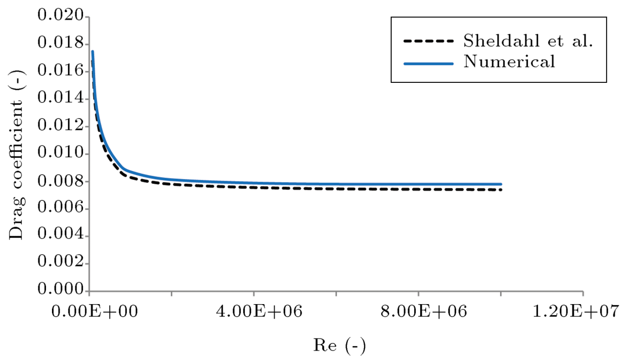

Figure 2. The variation of drag coefficient with respect to the Reynolds number ($\alpha = 4$).

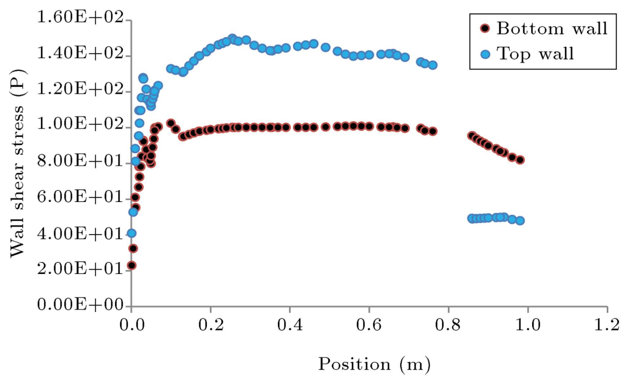

Figure 3. The variation of wall shear stress with respect to position for top and bottom walls (NACA 0015).

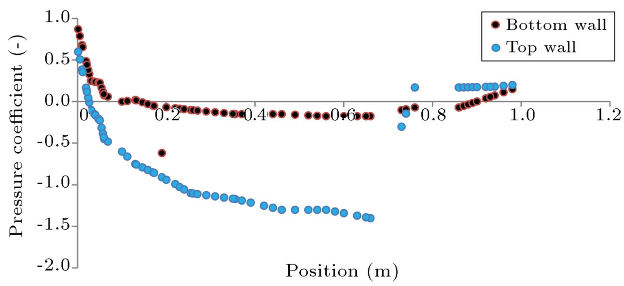

Figure 4. The variation of the pressure coefficient with respect to position for top and bottom walls (NACA 0015).

3.2. The pressure force around the airfoil NACA m1 for K-ε and S-A models

The results of the investigation on the pressure force around the airfoil NACA m1 with the angle of attack of zero for two turbulent models, K-ε and S-A, are shown in Figure 5. The results of the top wall show that by increasing the Mach number, the pressure force increases. Figure 6 shows the variation of the pressure force for the bottom wall of the airfoil. It has a similar trend with top wall. As it is seen from these figures, the maximum pressure force takes place around $M \approx 1$ for the Spalart-Almaras model, and it decreases up to $M \approx 1.05$ and increases after that value.

The outbreak of the shockwave phenomenon is shown in Figures 7 and 8, which are proving the exact location of the shockwave. Figures 7 and 8 show, respectively, the pressure coefficient and wall shear stress for the airfoil NACA m1, with respect to the position. As it is seen, the shock wave phenomenon takes place at the end of the top wall of the airfoil, which proves the exact location of this phenomenon for both pressure coefficient and wall shear stress. The pressure coefficient at the middle of the bottom wall of the airfoil is stable.

3.3. The viscous force around the airfoil NACA m1 for k-ε and S-A models

Figure 9 shows the viscous force on the top wall of the airfoil for k-ε and Spalart-Almaras models. A sudden dump is seen at $M \approx 1$ for Spalart-Almaras model, and after that, a slight decrease is occurring in the viscous force, but then the viscous force gets its increasing trend again. Figure 10 illustrates the viscous force at the bottom wall of the airfoil NACA m1 for Spalart-Almaras and k-ε models. A significant jump is seen in the bottom wall as well as the top wall. Figures 9 and 10 show that the viscous force at the bottom and top walls of the airfoil is approximately the same for different values of Mach number.

Figure 11 shows the total force around the airfoil NACA m1 for k-ε and Spalart-Almaras models for both top and bottom walls. The angle of the attack of the airfoil is 0°. As it is seen, the drag force has more values for Spalart-Almaras than the k-ε model. The most important difference between the two models

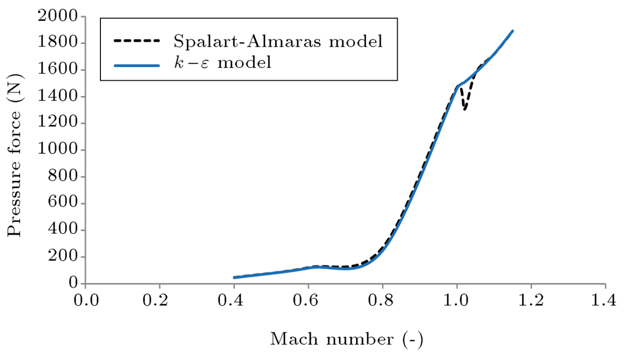

Figure 5. The variation of the pressure force with respect to Mach number for two models (top wall).

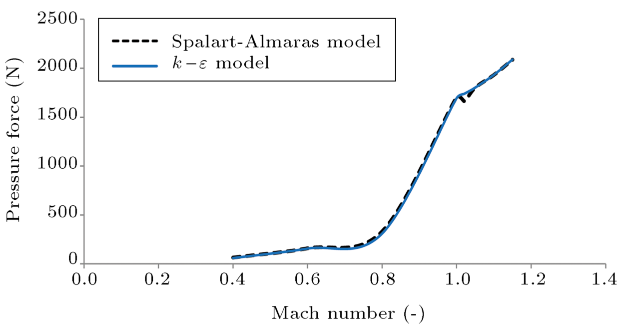

Figure 6. The variation of the pressure force with respect to Mach number for two models (bottom wall).

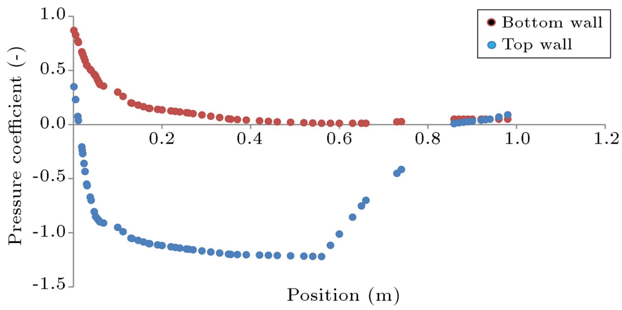

Figure 7. The pressure coefficient for the airfoil NACA m1 with respect to the position.

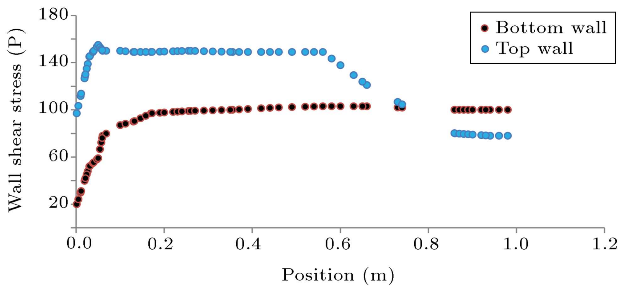

Figure 8. The wall shear stress for the airfoil NACA m1 with respect to the position.

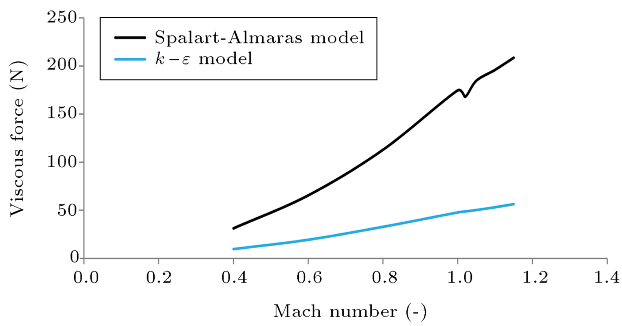

Figure 9. The variation of the viscous force with respect to the Mach number for the airfoil NACA m1 (top wall).

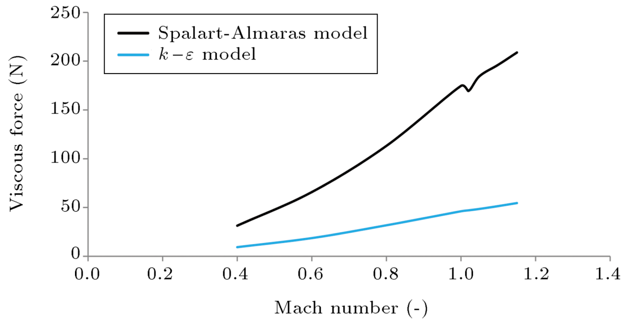

Figure 10. The variation of the viscous force with respect to the Mach number for the airfoil NACA m1 (bottom wall).

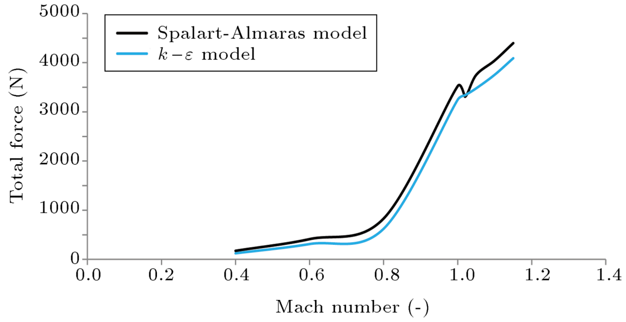

Figure 11. The variation of the drag force with respect to the Mach number for NACA m1.

is the viscous force due to significant importance of turbulence models on it; the viscous force has almost negligible values in k-ε model. The drag force has a significant jumping in $M \approx 1$ for both k-ε and Spalart-Almaras models.

3.4. The effect of the drag coefficient on the airfoil NACA m1 for the k-ε and S-A models

Figure 12 illustrates the variation of the drag coefficient against the Mach number for k-ε and Spalart-Almaras models. As it is seen, the Spalart-Almaras model anticipates more values of the drag coefficient in comparison with k-ε model. It shows that the highest value of the drag coefficient is occurred at $M \approx 1$. It is obvious that the drag coefficient has a sudden jump at $M \approx 1$ for both k-ε and Spalart-Almaras models, which shows the critical state at this point. The diagram has a slight drop after $M \approx 1$ for both k-ε and Spalart-Almaras models, but after that point, it has a stable trend.

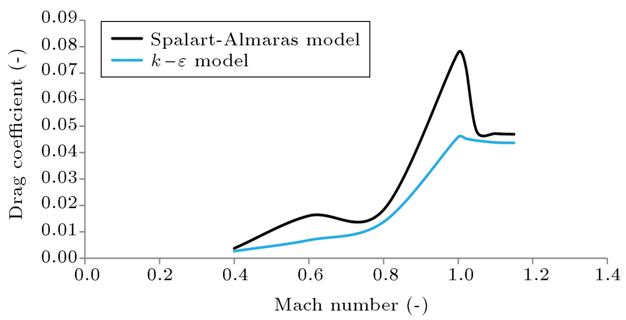

Figure 12. The variation of the drag coefficient with respect to the Mach number for NACA m1.

Figure 13 illustrates the pressure coefficients with respect to the Mach number for k-ε and S-A models. It is obvious that the pressure coefficient has the most effect on the drag coefficient.

3.5. Convergence criterion

The results of all cases were extracted after 800 iterations. As it is seen, the convergence was obtained after 400 iterations. The method which was employed in this study, for convergence, was coupled implicit. The coupled solver is recommended when dealing with applications involves high speed aerodynamics. The implicit solver will generally converge much faster than the explicit solver, but will use more memory. In this 2D case, memory is not an issue. The value of the convergence criterion for all of the cases was 10-3. Convergence will occur when the convergence criterion for each variable has been reached. The default criterion is that each residual will be reduced to a value of less than 10-3. The case which was used for the convergence criterion study was NACA m1 with Mach number of 0.8 and angle of attack of 40 which is illustrated in Figure 14.

4. Conclusion

- Thepressure force has experienced a sudden jump at $M = 1$ for the top and bottom wall of the airfoil,

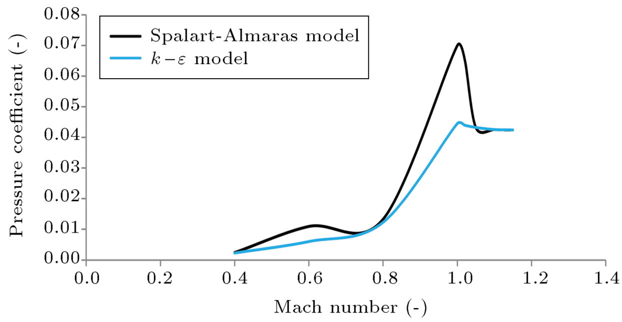

Figure 13. The variation of the pressure coefficient with respect to the Mach number for NACA m1.

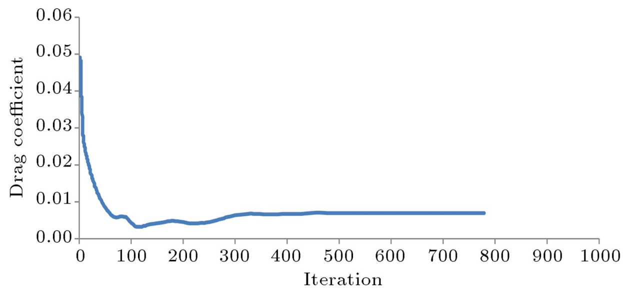

Figure 14. The drag coefficient with respect to the iteration in the convergence criterion study.

although the viscous force has not experienced such a decrease.

- The viscous force does not have a significant change in Spalart-Almaras model for the top and bottom wall of the airfoil.
- The viscous force does not have an important change in k-ε model too, but the viscous force have less values for both top and bottom walls of the airfoil in k-ε model in comparison with the S-A model.
- The viscous force has a considerable jump at $M = 1$ for top and bottom walls in the S-A model, whereas the viscous force does not experience a significant change for both top and bottom walls of the airfoil in k-ε model.
- The pressure and viscous forces have a slight decrease when $M = 1$ in both k-ε and S-A models, and after that value, they both increase again.
- The S-A model, in comparison with k-ε model, anticipates more drag forces around the airfoil, and the drag force has a considerable increase at $M = 1$ for both k-ε and S-A models.
- The S-A model predicts more drag coefficient than the k-ε model, and the drag coefficient has a significant rise for both models at $M = 1$; after this value, it has a stable state for both models.
- The pressure coefficient has the largest proportion in drag coefficient, although k-ε model predicts less drag coefficient.

References

1. Eriksson, L.E. and Rizzi, A. "Computer-aided analysis of the convergence to steady state of discrete approximations to the Euler equation", *J. Comput. Phys.*, **3**, pp. 57-90 (1985).
2. Van Buuren, R., Kuerten, J.G.M. and Geurts, B.J. "Instabilities of stationary inviscid compressible flow around an airfoil", *J. Comput. Phys.*, **138**, pp. 520-539 (1997).
3. Mittal, S. "Finite element computation of unsteady viscous compressible flows", *J. Comput. Methods Appl. Mech. Engrg.*, **157**, pp. 151-175 (1998).
4. Olejniczak, J. and Lyrintzis, A.S. "Design of optimized airfoils in subcritical flows", *J. Aircraft*, **31**, pp. 210-225 (1994).
5. Benard, N., Jolibois, J. and Moreau, E. "Lift and drag performances of an axisymmetric airfoil controlled by plasma actuator", *J. Electrostatics*, **67**, pp. 133-139 (2009).
6. Xuguo, Q., Peiqing, L., Qiulin, Q. "Aerodynamics of a multi-element airfoil near ground', *Tsingha Singhua Science and Technology*, **14**(S2), pp. 94-99 (December 2009).
7. Mittal, S. and Saxena, P. "Hysteresis in flow past a NACA 0012 airfoil", *Comput. Methods Appl. Mech. Engrg.*, **191**, pp. 2179-2189 (2002).
8. Rajakumar, S. and Ravindran, D. "Iterative approach for optimizing coefficient of power, coefficient of lift and drag of wind turbine rotor", *Renewable Energy*, **38**, pp. 83-93 (2012).
9. Shan, H., Jiang, L. and Liu, C. "Direct numerical simulation of flow separation around a NACA 0012 airfoils", *Computers and Flows*, **34**, pp. 1096-1114 (2005).
10. Zhou, Y., Alam, M., Yang, H.X., Guo, H. and Wood, D.H. "Fluid forces on a very low Reynolds number airfoil and their prediction", *Int. J. Heat and Fluid Flow*, **32**, pp. 329-339 (2011).
11. Ghadimi, P., Rostami, A.B. and Jafarkazemi, F. "Aerodynamic analysis of the boundary layer region of symmetric airfoils at ground proximity", *Aerospace Science Technology*, **17**, pp. 7-20 (2012).
12. Wang, S., Ingham, D.B., Pourkashanian, M. and Tao, Z. "Numerical investigations on dynamic stall of low Reynolds number flow around oscillating airfoils", *Computers and Fluids*, **39**, pp. 1529-1541 (2010).
13. Yao, J., Yuan, W., Wang, J., Xie, J., Zhon, H., Peng, M. and Sun, Y. "Numerical simulation of aerodynamic performance for two dimensional wind turbine wirfoils", *Procedia Engineering*, **31**, pp. 80-86 (2012).
14. Shi, S., Liu, Y. and Chen, J. "An experimental study of flow around a bi-inspired airfoil at Reynolds number $2.0^{*}10^{3}$", *J. Hydroudynamics*, Ser. B, **24**, pp. 410-419 (2012).
15. Medjroubi, W, Stoevesandt, B, Carmo, B. and Peinke, J. "High-order numerical simulation of the flow around a heaving airfoil", *Computers and Fluids*, **51**, pp. 68-84 (2011).
16. Spalart, P. and Allmaras, S. "A one-equation turbulence model for aerodynamic flows", American Institute of Aeronautics and Astronautics, Technical Report AIAA-92-0439 (1992).
17. Anderson, J., *Fundamentals of Aerodynamics*, McGraw-Hill, 3rd Ed., pp. 278-358, New York, US (1984).
18. Launder, B.E. and Spalding, D.B., *Lectures in Mathematical Models of Turbulence*, Academic Press, 1st Ed., pp. 1-270, London, England (1972).
19. Komerath, N. "AE 6020 compressible flow", University Course, George Institute of Technology, 1st Ed., pp. 1-60, Atlanta, US (2008).
20. www.aerolab.virtualave.net
21. Sheldahl, R.E. and Klimas, P.C. "Aerodynamic characteristics of seven airfoil sections through 180 degrees angle of attach for use in aerodynamic analysis of vertical axis wind turbines", SAND 80-2114, Sandia National Laboratories Albuquerque, New Mexico (1981).

Biographies

Sasan Akbarpour, MSc, was born in Tabriz, Iran, in 1985. He received his BSc degree in Mechanical Engineering from Islamic Azad University, Tabriz Branch, Tabriz, Iran, in 2009, and his MSc degree in Mechanical Engineering (Vehicle Propulsion Systems) from Sahand University of Technology, Tabriz, Iran in 2011. His areas of interest are diesel injection engines, HCCI engines, flows around the airfoils and CFD.

Morteza Ghorbani, MSc, was born in Tabriz, Iran, in 1986. He received his BSc degree in Mechanical Engineering from Islamic Azad University, Tabriz Branch, Tabriz, Iran, in 2009, and his MSc degree in Mechanical Engineering (Energy Conversion) from the Islamic Azad University, Takestan Branch, Takestan, Iran, in 2011. His areas of interest are bubble dynamics, multiphase flows in micro channels, flow regimes in nozzles and study on diesel engines primary breakup and spray characteristics. At present, he is a research Assistant at Center for CFD Studies on Heat Engines, Cavitational Flows and Petroleum Industries, Department of Mechanical Engineering at the University of Tabriz, Tabriz, Iran.